Soft Matter

PAPER

View Article Online
View Journal | View Issue

Cite this: *Soft Matter*, 2023, **19**, 1363

Formation kinetics and physicochemical properties of mesoscopic Alpha-Synuclein assemblies modulated by sodium chloride and a distinct pulsed electric field†

Mengying Wang,[a] Roland Thuenauer,[bcd] Robin Schubert,[e] Susanna Gevorgyan,[a] Kristina Lorenzen,[e] Hévila Brognaro[a] and Christian Betzel*[a]

Alpha-Synuclein (ASN), a presynaptic protein, has been widely reported to form amyloid-rich hydrogel clusters through liquid–liquid phase separation (LLPS) and liquid-to-solid transition. However, in-depth investigations about the parameters that influence the assembling kinetics, structures, and physicochemical properties of intermediate ASN assemblies are still missing. Therefore, we monitored for the first time the assembling and ordering kinetics of ASN by polarized/depolarized light scattering (DLS/DDLS) under the effect of ionic strength and a pulsed electric field (EF), followed by characterizing the resultant ASN assemblies applying thermostability assays, fluorescence/autofluorescence assays, and TEM. The underlying molecular mechanism was discussed based on experimental evidence. Results showed that in the presence of 150–250 mM NaCl, monomeric ASN is highly soluble in a temperature range of 20–70 °C and could form dissoluble liquid dense clusters *via* LLPS in crowded environments, while the ionic strength of 50 mM NaCl could trigger conformational changes and attractive diffusion interactions of ASN monomers towards the formation of mesoscopic assemblies with ordered internal structures and high thermostabilities. We discovered that pulsed EFs and ionic strength can modulate effectively the thermostability and autofluorescence effect of mesoscopic ASN assemblies by tuning the molecular interaction and arrangement. Remarkably, a specie of thermostable ASN assemblies showing a maximum autofluorescence emission at approx. 700 nm was synthesized applying 250 mM NaCl and the distinct pulsed EF, which could be attributed to the increase of β-sheet structures and hydrogen-bond networks within ASN assemblies. In summary, the presented data provide novel insights for modulating the growth kinetics, structures, and physicochemical properties of bio-macromolecular mesoscopic assemblies.

Received 8th December 2022,
Accepted 21st January 2023

DOI: 10.1039/d2sm01615j

rsc.li/soft-matter-journal

Introduction

Alpha-Synuclein (ASN) is an aggregation-prone protein, whose physiological function covers maintaining lipid-packing, sensing, and vesicle fusion.[1–4] Fibrillar aggregates of ASN have been widely detected in the nerve tissue of Parkinson's patients.[5–9] It was demonstrated that ASN undergoes liquid–liquid phase separation (LLPS) and liquid-to-solid transition before forming amyloid fibrils.[10] Recently, Sawner and Ray *et al.* (2021) have investigated and published the influence of pH, salt, PD-associated multivalent cations, N-terminal acetylation on the critical time and critical concentration of ASN LLPS *in vitro* applying PEG8000.[11] Monomeric ASN is a natively unfolded protein and can adapt a number of conformational states, caused by different intramolecular interactions in varying physicochemical environments.[12] The intramolecular interactions depend on electrostatic/hydrophobic interactions and hydrogen bonds between amino acid residues.[13] As a result, altering the physicochemical parameters, such as pH, salt, temperature, and external fields, can induce conformational changes in monomeric ASN and in ASN assemblies. The aggregation mechanism and the early stages of ASN fibrils have been investigated for many years. Krishnan and collaborators found in

[a] *University of Hamburg, Laboratory for Structural Biology of Infection and Inflammation, Institute of Biochemistry and Molecular Biology, Notkestrasse 85, c/o DESY, Building 22a, 22607, Hamburg, Germany. E-mail: christian.betzel@uni-hamburg.de*
[b] *Technology Platform Light Microscopy, University of Hamburg, Mittelweg 177, 20148, Hamburg, Germany*
[c] *Center for Structural Systems Biology (CSSB), Notkestrasse 85, c/o DESY, Building 15, 22607, Hamburg, Germany*
[d] *Technology Platform Microscopy and Image Analysis (TP MIA), Leibniz Institute of Virology (LIV), Martinistrasse 52, 20251, Hamburg, Germany*
[e] *European XFEL GmbH, Holzkoppel 4, 22869, Schenefeld, Germany*
† Electronic supplementary information (ESI) available. See DOI: https://doi.org/10.1039/d2sm01615j

2003 that the formation of an ASN dimer is the critical step for fibrillation,[6] while in 2008 Tashiro's group, using time-resolved SAXS, detected an oligomerized heptamer at the initial stage of ASN fibrillation.[14] Applying dynamic light scattering, Saraiva (2021) identified micellar-like aggregates with hydrodynamic radii (R_h) of approx. 210 nm at low concentrations of ASN (<100 μM) and oligomers with R_h approx. 82 nm at high protein concentrations (>100 μM) in the early stages of aggregation.[15] Especially, the metastable globular oligomers have been observed widely preceding the formation of rigid fibrils as protofibrils.[16–19] On the other hand, using both amyloid-β and lysozyme, Hasecke *et al.* (2018) revealed that the fibril assembling kinetics depends on the critical oligomer concentration and suggested that the globular oligomers can compete with the fibrils consuming monomeric proteins, thus inhibiting the nucleation and growth of rigid fibrils.[20] Obviously, the interconvertibility among ASN monomers, dimers, oligomers, and fibrils highly depends on the physicochemical conditions.

It was reported that an electric field (EF) strength across the neuron synapses is approx. 40 kV cm^{-1},[21] which can cause the self-aggregation of proteins. In this context, the role of EFs in the assembling process of ASN and the physicochemical properties of intermediate ASN assemblies are till now not studied. Therefore, in the data we present and corresponding experiments performed, we focus on gaining insights into the effect of physicochemical factors, EFs and a NaCl gradient, on the early-stage assembling mechanism of ASN and the physicochemical properties of ASN intermediate assemblies. The experimental strategy is shown in Scheme 1. Polarized, and depolarized dynamic light scattering (DLS/DDLS) were employed to monitor simultaneously the early-stage evolution of the hydrodynamic radius and anisotropy of ASN assemblies. A light scattering instrument installed with a temperature control program was utilized to analyse the thermostability of monomeric ASN and the interconvertibility between ASN assemblies, oligomers, and monomers. Transmission electron microscopy (TEM), optical brightfield microscopy, and confocal laser scanning microscopy (CLSM) were applied to characterize the morphologies and autofluorescence effect of ASN assemblies. Finally, the diffusion interaction parameter-K_D and the secondary structure of monomeric ASN under different conditions were also determined to uncover the underlying molecular mechanism resulting in the diverse phase behaviours of ASN.

Results and discussion

Phase diagram of α-Synuclein in solution at pH 7.4 and applying PEG8000 as a crowding agent

With the resolution of an optical microscope Leica M205C, ASN dense liquid clusters (DLCs) and mesoscopic globular assemblies (10–1000 nm) were observed from droplets incubated 1 hour in a sitting-drop plate at 20 °C and conditions shown in the dotted frame of Fig. 1. It was noticed that ASN at high concentrations (200–500 μM) tended to undergo liquid–liquid phase separation (LLPS) and form DLCs after 1 hour incubation with 10–20% PEG8000, followed by liquid to gel-like transitions within 72 hours of incubation (ESI† Fig. S2–S4). However, at low concentrations (5–100 μM) ASN mainly aggregated to globular mesoscopic assemblies within 1 hour of incubation applying 15–20% PEG8000 (Fig. 1). Similar phase diagram of ASN mixed with PEG8000 was also observed by Sawner's group[11] and Ray's lab.[22] ASN self-assemblies, without applying a crowding agent, were also observed after 24 hours of incubation (the first column of ESI† Fig. S2). The mesoscopic assemblies have homogeneous dimensions regardless which protein concentration was applied. Further, fibrillar structures formed *via* the linear attachment of mesoscopic globular assemblies were observed in droplets containing 50–100 μM ASN and PEG8000 after 24 hours of incubation (ESI† Fig. S2–S4), which can be considered to be the origin of fibrillation.

Monitoring the dynamic assembling and three dimensional (3D)-ordering of α-Synuclein in a NaCl gradient exposed to pulsed EFs

To obtain insights about the early-stage assembling and 3D-ordering kinetics of ASN, a non-invasive DLS/DDLS technique

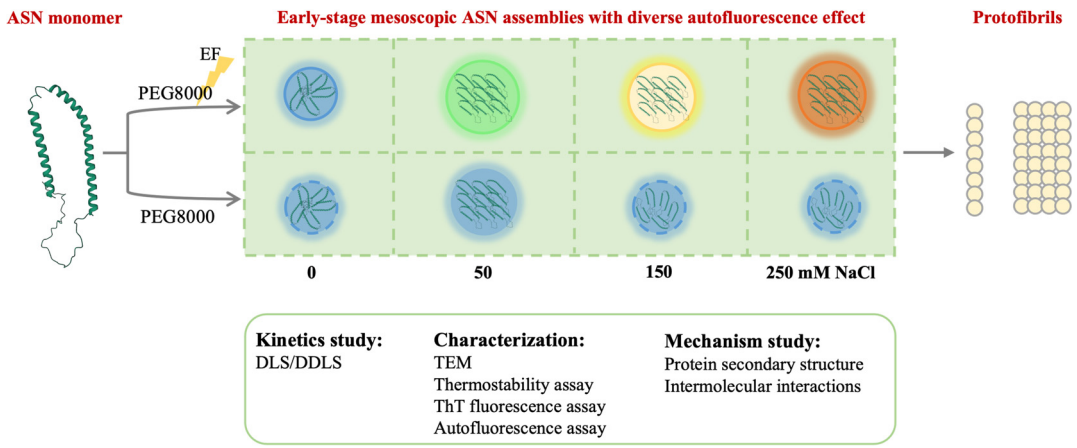

Scheme 1 Experimental strategy. The coordinates of monomeric α-Synuclein (ASN) were obtained from the protein data bank (PDB code: 2KKW).[40] The colour of mesoscopic assemblies denotes the diverse autofluorescence effects. The molecular arrangement shown in different assemblies do not represent the real inner structure of ASN assemblies.

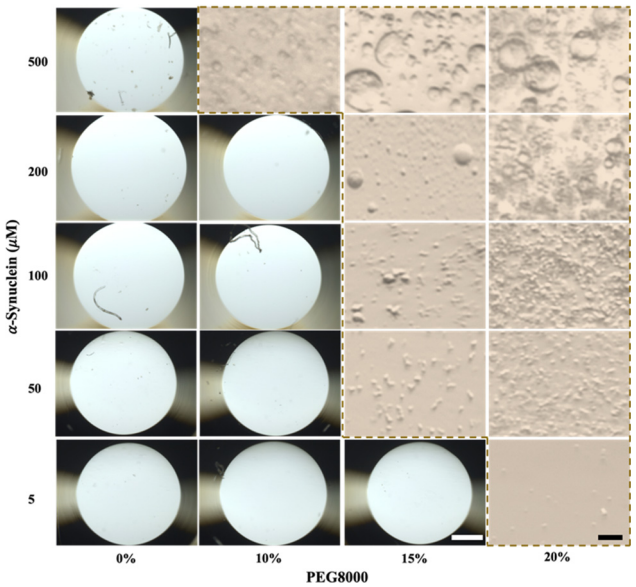

Fig. 1 Representative phase diagram of α-Synuclein after 1 hour incubation applying PEG8000 in a buffer of 20 mM Tris pH 7.4, 150 mM NaCl and 1 mM DTT at 20 °C. The white scale bar corresponds to 50 μm for all droplets, while the black scale bar represents 10 μm for all magnified images shown in the dotted frame.

monitoring simultaneously and time-resolved the hydrodynamic radii and optical anisotropy of particles was utilized. Firstly, ASN solutions applying NaCl in a range of 0–250 mM and pH 7.4 were investigated at 20 °C to understand the effect of NaCl and the applied EF on ASN stabilities and self-assembling behaviour. As a sufficient DLS signal intensity is required for generating a normal autocorrelation function to analyse the particle radii, a concentration of 200 μM ASN was applied for the pure protein samples. Results showed that the monomeric ASN was stable within 2 hours of measurements at high concentrations of NaCl, 150–250 mM (the upper panel of Fig. 2a). However, oligomers with a hydrodynamic radius (R_h) of approx. 7.6 nm and 46.0 nm formed after 2 hours in solutions containing none NaCl, and 50 mM of NaCl, respectively.

The clustering evolution was also monitored in solutions containing 50 μM ASN, a physiological relevant ASN concentration, 15% PEG8000, and NaCl ranging from 0 up to 250 mM. Fig. 2b revealed the instant formation of ASN oligomers with R_h of approx. 20 nm in the absence, and the presence of 150–250 mM NaCl. Accordingly, the R_h growth kinetics of ASN oligomers in presence of 150–250 mM NaCl followed the scaling power law of $R_h = k \times t^{0,33}$, where k is a constant pre-factor and t is the time,[23] demonstrating a diffusion-limited Ostwald ripening mechanism of LLPS.[24] Despite the fact that the initial and final R_h of ASN assemblies obtained at 0 mM NaCl are comparable with assemblies obtained at 150–250 mM NaCl, the R_h developing pattern observed within 2 hours of measurements showed a power law of $t^{0,2}$ at 0 mM NaCl. The ionic strength of 50 mM NaCl favoured the largest ASN assemblies with R_h approx. 100 nm appearing and growing with the power law of $R_h = k \times t^{0,5}$, implying a surface attachment-limited coarsening.[23] It's worth noting that the growth of ASN R_h from 100 to 500 nm in 18 minutes was accompanied by the descent of the corresponding DLS signal intensity (purple circles) and an increase of the DDLS signal intensity (green rhombuses) (Fig. 2b). Considering that the DLS signal intensity depends on the particle size and concentration,[25] thus the reducing DLS signal intensity indicated that parts of metastable mesoscopic assemblies formed at the beginning of mixing and were consumed during the growth and ordering of ASN assemblies. Both, DLS and DDLS signal intensities reached a plateau after 18 minutes, considering the continuous growth of R_h, it indicates an equilibrium between the growth in size and the decrease in the number of ASN assemblies. Fig. 2c and d are displaying the evolving results of ASN in the same solutions, as shown in Fig. 2a and b, respectively, but under the influence of a pulsed electric field (EF) applied throughout during the measurement. Compared to the corresponding control groups, it is apparent that EFs prompted the formation of ANS assemblies with a slight anisotropy in the absence of PEG8000. According to the R_h growth pattern and DLS/DDLS signal intensities obtained for the control and EF experiments we showed that EF cannot influence the phase behaviour of ASN in a PEG8000 solution without the presence of ions (Fig. 2b and d, 0 mM NaCl). However, the applied EF modified the early-stage phase behaviours of ASN in PEG8000 solutions containing 50–250 mM NaCl, since the obtained R_h data did not fit to the scaling power law of both the surface attachment-limited coarsening ($t^{0,5}$) and the diffusion-limited Ostwald ripening ($t^{0,33}$) mechanisms (Fig. 2d, 50–250 mM NaCl). The DDLS signal intensities of EF groups at 150–250 mM NaCl were stronger than their corresponding control groups, suggesting a more ordered alignment of ASN molecules, guided by the applied EF. To analyse further the effect of NaCl and applied EF on physicochemical properties of ASN assemblies and considering the visible particle dimension, samples, presented in Fig. 2b and d, were characterized by TEM and optical microscopy, as summarized below.

Characterizing the morphologies and β-sheet structures of assembled α-Synuclein at different time scale

To track the morphological transitions of ASN assemblies considering a physiological relevant protein concentration of 50 μM,[26,27] samples shown in Fig. 2b and d were incubated at 20 °C for 3 days and analysed afterwards by TEM. Results showed that mesoscopic ASN assemblies formed in control groups without EFs showed mainly a globular shape (upper row of Fig. 3a), whereas aggregated assemblies were also observed in EF groups (lower row of Fig. 3a). Especially, protofibril-like morphologies formed through curvilinear or linear attachment of globular assemblies were detected in EF groups containing 0 and 50 mM NaCl, respectively. Thioflavin T (ThT), which increases the fluorescence intensity upon binding to amyloid β sheets, was used to analyse the fibrillation of ASN assemblies. In accordance with the DDLS results about the internal structure changes, ASN assemblies in the EF group containing 150 or 250 mM NaCl exhibited a higher fluorescence intensity than the control group, while no noticeable difference was detected between the control and EF groups at solution conditions of 0–50 mM NaCl (Fig. 3b). It was reported that Congo red (CR) dye specifically stains stacked β-sheet aggregates and

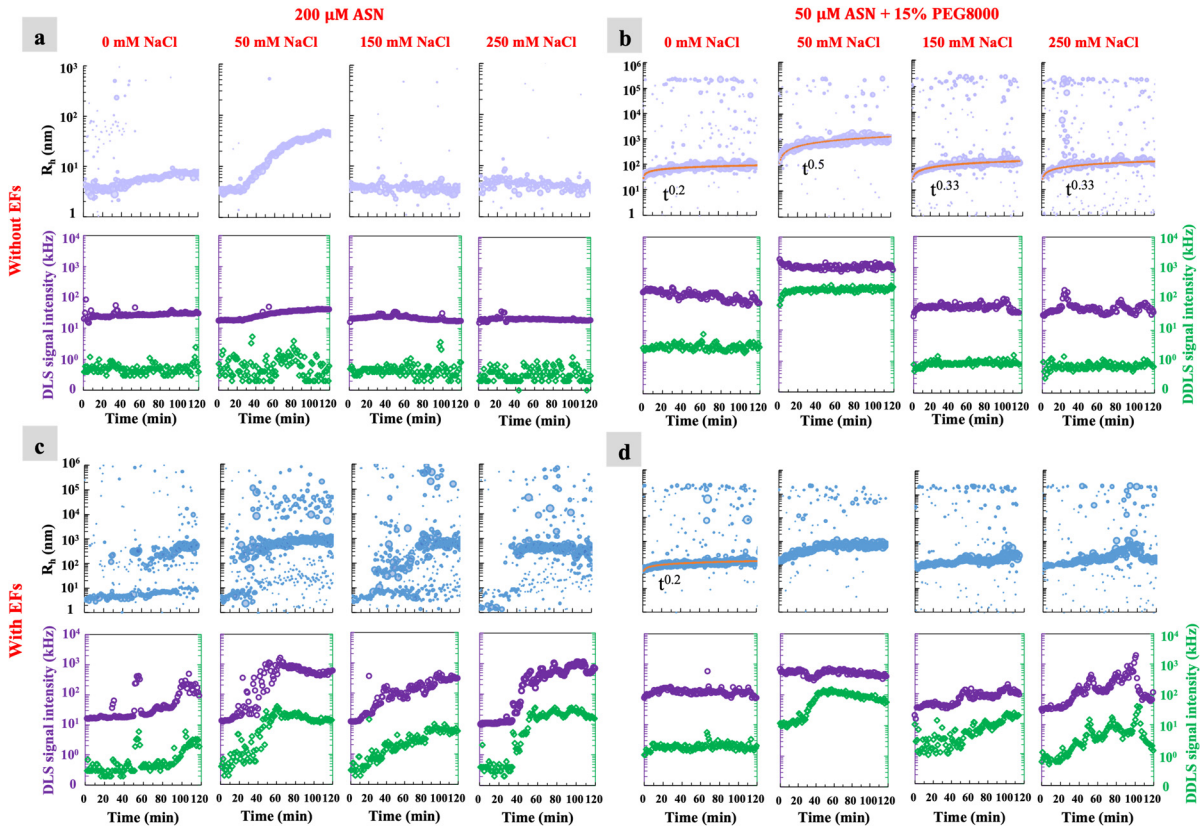

Fig. 2 The dynamic evolution of hydrodynamic radii and internal order during the early stage assembling of α-Synuclein applying a NaCl gradient and pulsed EFs. 200 μM of α-Synuclein solutions containing a gradient of NaCl from 0 up to 250 mM (a) without and (c) with the application of EFs. Mixtures of 50 μM α-Synuclein with 15% PEG8000 and NaCl range of 0–250 mM (b) without and (d) with the stimulus of EFs. All solutions are in 20 mM Tris–HCl buffer at pH 7.4 and containing 1 mM DTT. The DLS (purple circles) and DDLS (green rhombuses) signal intensities detected from each condition were plotted below the corresponding hydrodynamic radii graph.

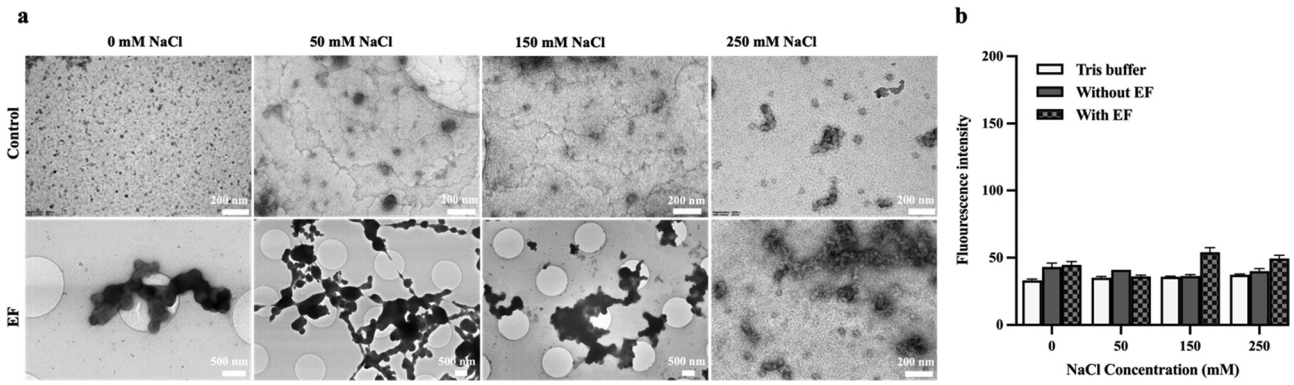

Fig. 3 (a) TEM images and (b) ThT fluorescence assays of ASN assemblies incubated at 20 °C for 3 days in solutions of 50 μM ASN, 15% PEG8000, and a NaCl gradient in the absence (control) or being exposed for 2 hours by a pulsed electric field.

does not bind to non-polymerized amyloid peptides.[28–30] Therefore, 0.01% (w/v) CR was added to the solutions containing 50 μM ASN and 15% PEG8000 to detect stacked β-sheet structure elements. As presented in ESI† Fig. S5a, monodisperse globular ASN assemblies showed the same colour as the surrounding solution. Nonetheless, the aggregated assemblies showed a more intensive colour of CR dye than the solvent, demonstrating the presence of stacked β sheets inside the aggregated ASN assemblies. ESI† Fig. S5b displayed the CR staining results for the eight ASN samples prepared applying the same procedure as for the samples used for TEM and ThT assays. Except for globular ASN assemblies observed in the control group with solution conditions containing 50–250 mM NaCl, aggregated ASN assemblies formed in all other groups showed a strong binding of the CR

dye, revealing the formation of stacked β sheets within ASN assemblies.

After a continuous incubation of samples displayed in Fig. 2b and d for 30 days, mesoscopic globular ASN assemblies appeared to aggregate with each other particular in control groups having 0–50 mM NaCl in the solution and in all EF groups (Fig. 4a). Remarkably, the ordered arrangement of globular assemblies within the aggregated structure is particularly discernible in the control group at 50 mM NaCl and in the EF group containing 250 mM NaCl (Fig. 4a), which also exhibited relatively high fluorescence intensities applying the ThT assay (Fig. 4b). According to the DDLS results (Fig. 2), optical anisotropy was detected for early-stage ASN mesoscopic assemblies formed in the control group applying 50 mM NaCl and in the EF group applying 250 mM NaCl. Thus, we presume that the driving force for ASN mesoscopic assemblies attaching to each other to form larger aggregated structures with internal order might be attributed to the early-stage nucleation.

Characterizing the thermostability of monomeric and assembled α-Synuclein

The thermostability of ASN monomers was analysed in solutions containing different NaCl concentrations (0, 50, 150, and 250 mM) along with a temperature ramp up (purple circles in Fig. 5) and subsequently ramp down (green circles). Results demonstrated that monomeric ASN with R_h of approx. 3.6 nm in solutions applying 150–250 mM NaCl is highly soluble in the temperature range of 20–70 °C (Fig. 5a). On the other hand, irreversible and stable ASN oligomerization was observed after the temperature ramp down in solutions containing 0–50 mM NaCl.

Mesoscopic ASN assemblies formed after 2 hour incubation in presence of NaCl and PEG8000 were also monitored in the solution along the temperature ramping (Fig. 5b) and demonstrated a temperature dependency in the presence of 0, 150, and 250 mM NaCl, which reveals weaker bonding forces of attraction among the ASN clusters. The reversible ability meets well with the property of liquid dense clusters formed *via* LLPS, for which the kinetics is shown in Fig. 2b.

Further, highly thermostable ASN assemblies, formed in the presence of pulsed EFs during 2 hour incubation, were detected in the temperature ramp experiment applying all NaCl conditions, as mentioned before (Fig. 5c). Also, the thermostability observed for the mesoscopic assemblies of ASN containing 50 mM NaCl without applying EFs (Fig. 5b) corroborates well with the DDLS results and confirmed that changes in the optical properties of the colloidal material are related to the formation of a geometrically ordered molecular arrangement within ASN assemblies (Fig. 2b, 50 mM NaCl). In conclusion, ASN monomers are more thermostable at higher NaCl concentrations (150–250 mM), while ordered mesoscopic ASN assemblies are more resistant to higher temperature than the disordered DLCs. The regularization of the ACF fitting curves at different temperatures are shown for each condition in ESI† Fig. S6.

Characterizing the autofluorescence effect of α-Synuclein assemblies

It is reported that the aromatic amino acid residues tyrosine, phenylalanine and tryptophan exhibit intrinsic fluorescence with both excitation and emission in the UV range of 260–280 nm.[31] However, amyloid fibrils specifically emit fluorescence in the visible spectra range of 400–450 nm because of the electron delocalization in the hydrogen-bond-rich network of fibrils.[31–33] It is also observed that dityrosine can emit fluorescence in the range of 400–420 nm upon excitation at 284 nm or 315 nm, due to noncovalent π–π stacking between tyrosine residues.[34] ASN contains two phenylalanine and four tyrosine amino acids. Therefore, to avoid the contribution of aromatic amino acid residues to the autofluorescence intensity, we analysed the autofluorescence effect of ASN assemblies within the emission spectra range of 420–780 nm applying an excitation wavelength of 405 nm utilizing a confocal laser scanning microscopy (CLSM). The CLSM brightfield images (Fig. 6a) and autofluorescence images (Fig. 6b) showed early-stage morphologies of ASN assemblies formed in solutions within 2 hours at 20 °C.

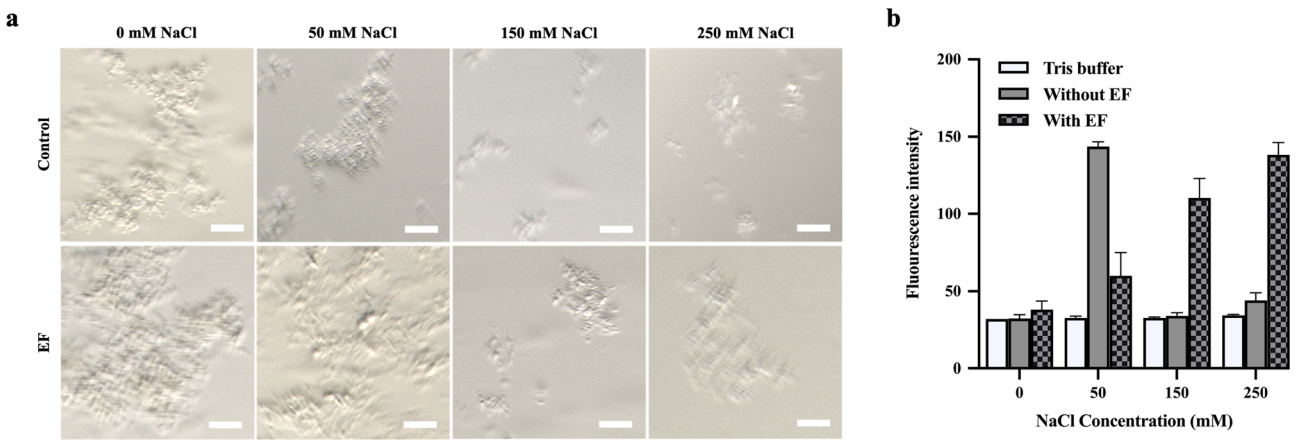

Fig. 4 (a) Optical brightfield microscopy images and (b) ThT fluorescence assays of 50 μM α-Synuclein incubated with 15% PEG8000 and applying a NaCl gradient for 30 days at 20 °C, in the absence (control) or being exposed for 2 hours by a pulsed EF. Scale bars correspond to 20 μm.

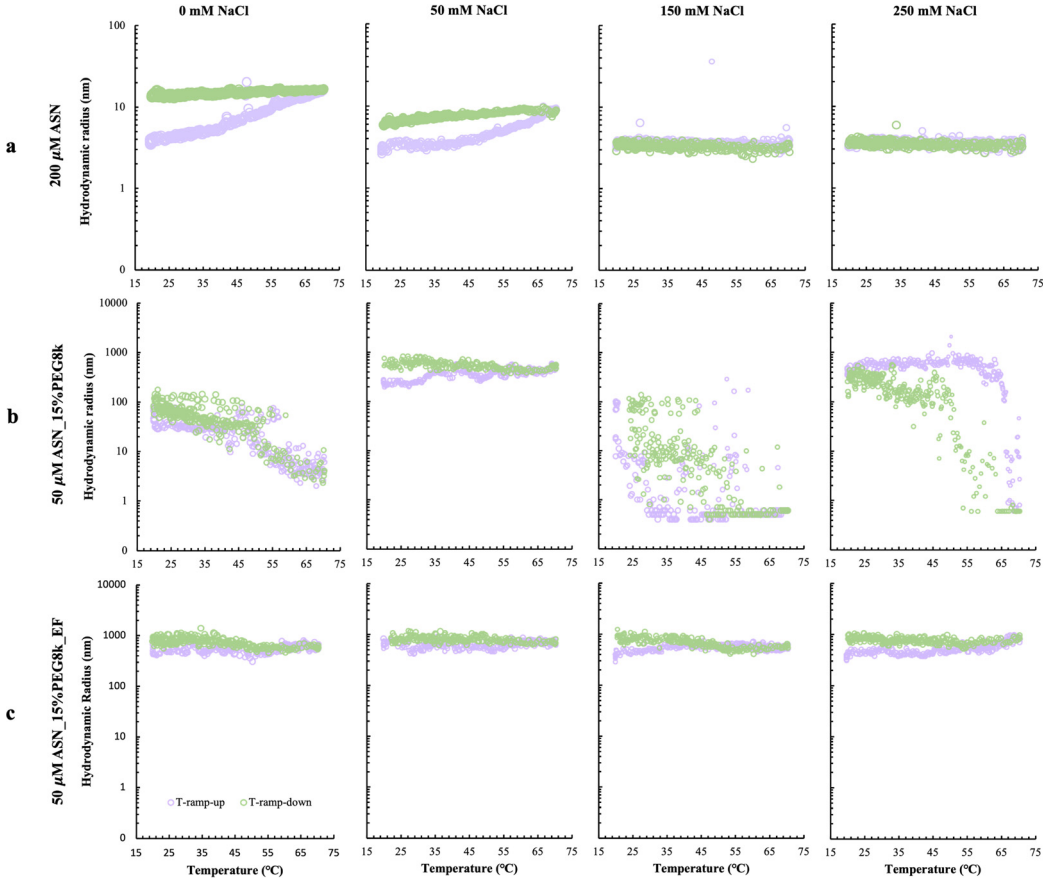

Fig. 5 The thermostability of (a) monomeric ASN, and the reversibility of assembled ASN induced by PEG8000 after 2 hours (b) without and (c) with a pulsed EF exposing to the solutions containing 20 mM Tris buffer pH 7.4 and a NaCl gradient.

Identical aforementioned conditions were applied in the presence and the absence (control group) of EFs. Consistent with TEM observations, mesoscopic ASN assemblies exhibited mainly monodisperse, globular, and relatively homogeneous dimension in the solution of the control group (upper rows of Fig. 6a and b), while under the effect of pulsed EFs the mesoscopic ASN assemblies packed up into an agglomerated arrangement (lower panels of Fig. 6a and b). The three-dimensional (3D) distribution of ASN assemblies in each solution were also analysed applying *in situ* 3D fluorescence scanning. The spatial distribution and the morphologies of ASN assemblies observed in the solution at different conditions are shown in ESI† Fig. S7.

The fluorescence emission spectra of ASN assemblies formed in the aforementioned conditions were also analysed. Results showed that mesoscopic ASN assemblies formed without applying EFs (control group) in all NaCl concentrations emitted a main peak with a maximum intensity at 470–490 nm, while the maximum emission spectrum of ASN assemblies, induced by pulsed EFs, presented a gradual red shift along with the increasing concentration of NaCl up to 250 mM (Fig. 6c). In the presence of EFs, applying 50 mM NaCl, a second minor peak at approx. 660 nm emerged in the spectrum and became more prominent at 150 mM NaCl, which two different electronic structures with emission spectrum peaks detected at 500 and 660 nm (Fig. 6c, 150 mM NaCl). Further, the maximum emission spectra of ASN assemblies formed in the presence of 250 mM NaCl and EFs completely red-shifted the spectrum to the wavelength range of 680–700 nm. In other words, only changing ionic strength cannot alter the optical properties of ASN assemblies, however, an ionic gradient can assist EFs to induce assemblies with diverse secondary structures formed in the ASN agglomerates.

Efforts have been made to red-shift the emission wavelength for bioimaging applications, as longer emission wavelengths have less damage to cells and can minimize the background absorption.[35] Therefore, mesoscopic ASN assemblies with red-light autofluorescence are very prospective to be applied as label-free bioimaging markers. Grelich-Mucha and collaborators have revealed in 2021 that the arrangement of β-sheet structures and the resultant hydrogen-bond patterns influence the autofluorescence of fibrils by comparing the structural and optical properties of twisted and tapelike fibrils.[36] Therefore, based on the data obtained by DDLS measurements (Fig. 2b and d) and ThT assays (Fig. 3b), which showed the internal order rearrangement and the composition of β-sheet structures within ASN assemblies according to the rise of NaCl concentration and the presence of pulsed EFs, we deduce that the red-shifted emission spectra of ASN assemblies could be attributed to the increased composition of β-sheet stacks and hydrogen-bond networks within ASN assemblies. It's worth noticing that assemblies formed at 50 mM NaCl and in the absence of EFs

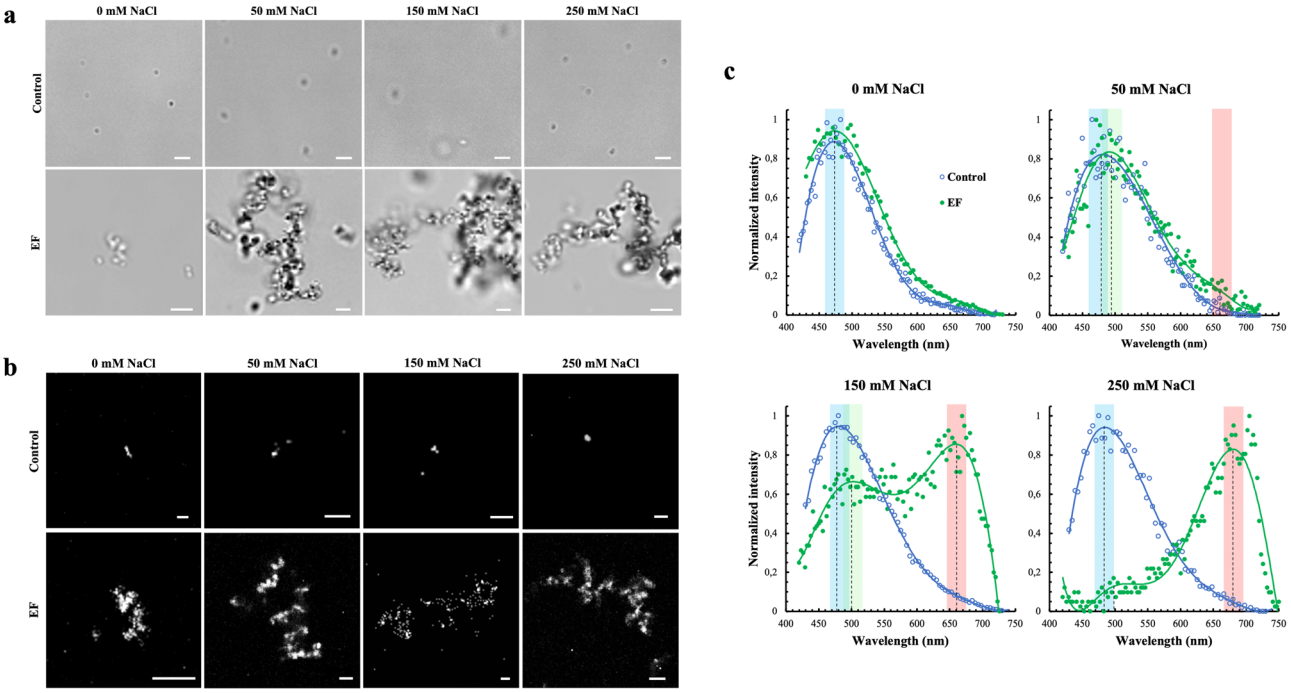

Fig. 6 (a) CLSM bright-field images of ASN assemblies observed after 2-hour incubation of 50 μM ASN with 15% PEG8000 in different NaCl solutions without (control group) or in presence of pulsed EFs at 20 °C. (b) The autofluorescence images and (c) corresponding normalized emission spectra upon excitation at 405 nm. Scale bars in figures a and b correspond to 2 μm. Blue circular symbols and green dots in each graph of figure c are showing the experimental data of ASN samples without (control) and with EF treatment, respectively, the solid line is the corresponding fitting curve for each experimental data set.

did not show a clear redshift, although orientation-dependent interactions were detected by DDLS. The low ThT fluorescent intensity (Fig. 3b) and the light CR colour (ESI† Fig. S5b) observed from ASN assemblies, incubated with 50 mM NaCl for 3 days, indicate that their internal molecular arrangement in early stages is different from the observed β-sheet structures induced by EFs.

Determination of the diffusion interaction parameter (K_D) and the secondary structure of monomeric α-Synuclein

To understand the molecular mechanism resulting in the diverse behaviours of ASN described before, the diffusion interaction parameter-K_D values and the secondary structure of ASN monomers were investigated.

K_D values. The parameter K_D indicates the protein diffusion interactions and can be determined by analysing the dependence of the diffusion coefficient in context of the protein concentration in solution. Positive K_D value reveals a repulsive diffusion interaction while negative K_D value denotes an attractive interaction among protein monomers. To analyse the effect of different NaCl concentrations on the molecular diffusion interactions of ASN, the diffusion coefficient of monomeric ASN at different protein concentrations were measured by DLS in solutions with NaCl ranging from 0 to 250 mM. K_D value was determined, based on Equation 3, for each solution and is shown in Fig. 7. Monomeric ASN in all NaCl solutions presented a negative K_D value indicating attractive diffusion interactions, which is probably caused by the intrinsic disordered structure of ASN. The ionic strength of 10 mM NaCl promoted the strongest attractive interaction among ASN monomers. Nonetheless, the increase of Na^+/Cl^- in the solution gradually raised the repulsive force and thus stabilized ASN molecules. This fact is also shown in Fig. 2a and 5a, since none ASN aggregation was observed in solutions with NaCl concentrations of 150 and 250 mM.

The secondary structure. The far-UV circular dichroism (CD) spectra of monomeric ASN in solutions containing 20 mM Tris buffer at pH 7.4 in the presence of a gradient of NaF were measured to study the ionic strength influence on the secondary structure of ASN. In this experiment NaCl was replaced by NaF because the chloride ions show strong absorption at wavelengths less than 195 nm. For each NaF concentration an ASN sample was pretreated by EFs for 1 hour and measured by CD to study the effect of EFs on the conformation of ASN. The full wavelength spectra (190–260 nm) of all ASN samples showed a main negative peak between 195 and 200 nm, which characterizes the secondary structure of random coils (Fig. 8a). A magnified view of the spectra of all samples in the range of 190 up to 210 nm exhibited a similar spectra profile with minor fluctuations in the region of the main peak, 195–200 nm. The only exception noticed was a second main peak maximum at a wavelength of 191–192 nm for a ASN solution containing 50 mM NaF without applying a pulsed EF (green dashed line in Fig. 8b).

After analysing the results described above, one question became nonnegligible: why 50 mM NaCl showed distinct effect on the conformation and phase behaviour of ASN although ASN

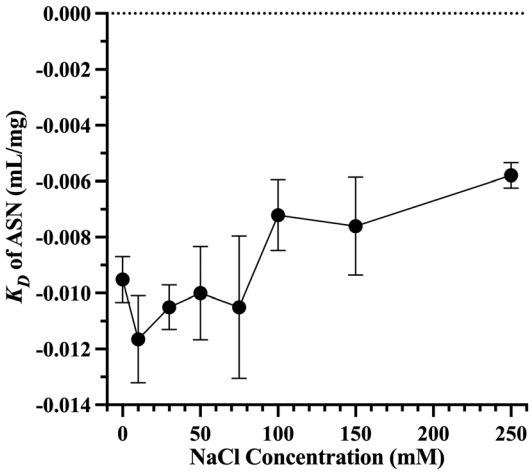

Fig. 7 The determined diffusion interaction parameter—K_D value of ASN in solutions with Tris buffer pH 7.4 and varied NaCl concentrations.

K_D values at 0 and 50 mM NaCl are similar? Recently, Ubbiali *et al.* showed by applying cross-linking/mass spectrometry that the native ASN monomer can form a hairpin-like structure *via* the long-range interaction between the positively charged N-terminal region with the negatively charged C-terminal region, and can change to a more elongated structure after LLPS.[37] As an intrinsically disordered protein (IDP), ASN monomers can form intra- and inter-molecular interactions thus performing conformational transitions according to the environments. Based on our K_D results (Fig. 7), the intermolecular attraction of unfolded ASN induced by NaCl was maximum at 10 mM NaCl and gradually reduced upon increasing the NaCl concentration from 30 to 250 mM. Using the same methods, we have investigated previously the effect of NaCl on the diffusion interactions of the well folded protein glucose isomerase (GI) and showed that increasing NaCl within the range of 0–500 mM can constantly weaken the repulsive intermolecular interactions of GI.[38] Obviously, the charge screening effect of NaCl on unfolded ASN and well folded GI is different because of the surface accessible regions of the protein. For well folded proteins, the monovalent ions mainly modulate the surface net charge thus the electrostatic interactions; But for unfolded IDPs, ions can access most of the protein domains to influence not only inter- but also intra-molecular interactions thus resulting in the conformational transition and the nonlinear dependence of the intermolecular interactions of ASN on ionic concentration (Fig. 7). We confirmed that the charge screening effect of 50 mM NaCl on ANS induced a specific conformation (Fig. 8) which favours protein–protein interactions towards the formation of ordered mesoscopic ASN assemblies (Fig. 2b) and β-sheet structure (Fig. 4). Based on those data, now we can also understand the different morphologies of ASN mesoscopic assemblies induced by EF at different NaCl conditions, as shown in Fig. 3a. Demonstrated by the DDLS results, shown in Fig. 2d, different internal ordering was detected for mesoscopic assemblies of ASN formed at different NaCl concentrations. ASN monomers can elongate to distinct conformations upon interacting and forming mesoscopic assemblies with different structures, as observed by TEM from ASN samples incubated for 3 days (Fig. 3a).

Another nonnegligible question came up from the observed phenomena is: why EF showed different influential trend on the later organization (Fig. 4a) and fibrillation level (Fig. 4b) of mesoscopic ASN assemblies induced at different NaCl concentrations? Recently, it was reported that the critical size of ASN oligomers/assemblies capable to form stable fibrils is approx. 40 nm.[39] Our data showed that ASN self-assemblies with R_h of approx. 46 nm formed at 50 mM NaCl within 2 hours (Fig. 2a, 50 mM NaCl) thereby revealed the interaction propensity of ASN towards fibrillation, which was subsequently validated by DDLS indicating significant internal order (Fig. 2b, 50 mM NaCl), higher thermostability (Fig. 5b, 50 mM NaCl), and stronger ThT fluorescence intensity (Fig. 4, 50 mM NaCl). On the other hand, the R_h (Fig. 2a and 5a, 150–250 mM NaCl) and lower K_D values (Fig. 7) unveiled that ASN monomers have relatively weak interactions at 150–250 mM NaCl, resulting in a smaller number of disordered ASN assemblies with lower

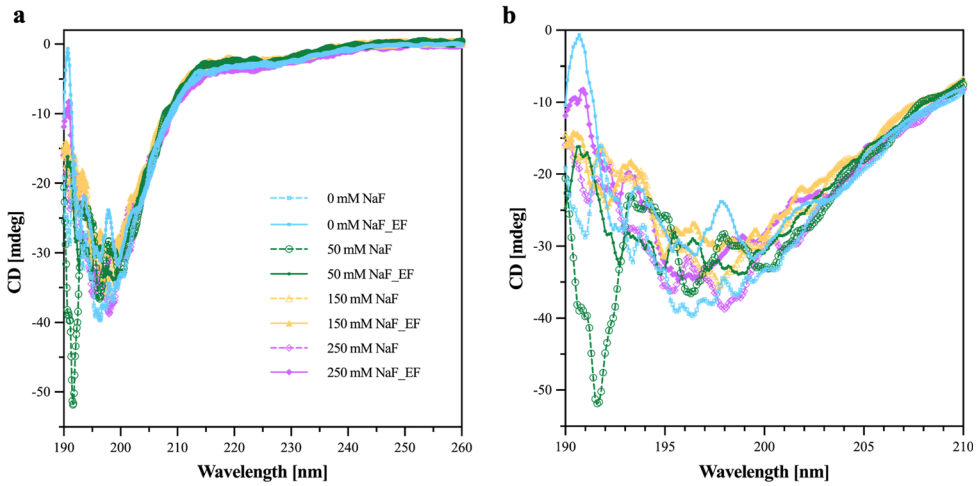

Fig. 8 The far-UV CD spectra of ASN (0.2 mg mL^{-1}) without and with the effect of EFs in solutions containing a gradient of NaF (0–250 mM). (a) The full-wavelength far-UV CD spectra of ASN. (b) Magnified view of the ASN CD spectra in the wavelength range of 190–210 nm.

thermostability (Fig. 2b and 5b, 150–250 mM NaCl). The effect of the applied EF on ASN organization was supported by increasing NaCl concentrations (Fig. 2, 4, and 6c). The only exception is that the optical anisotropy level of ASN mesoscopic assemblies formed at 50 mM NaCl and applying EF (DDLS signal intensities in Fig. 2d, 50 mM NaCl) and the later observed fibrillation (Fig. 4b, 50 mM NaCl) reduced compared to the corresponding control group. This can be explained by the CD results obtained (Fig. 8), as a specific conformational transition favouring fibrillation was induced by 50 mM NaCl, but was altered by EF. Thus, we conclude that the effect of pulsed EF on ASN assembling/fibrillation is reinforced by increasing the ionic strength, except for the case of particular conformational modulations induced by certain ionic concentrations.

Conclusion

We investigated the kinetics and physicochemical properties of ASN assemblies applying PEG8000 as a crowding agent at pH 7.4. Results obtained confirmed that ASN tended to undergo LLPS and form DLCs in crowded environments at relative high protein concentrations (>100 μM). However, it preferred to assemble oligomers or mesoscopic globular assemblies at low protein concentrations (<100 μM). The early-stage evolution of the dimensions and the internal arrangement of ASN assemblies was monitored applying a series of NaCl solutions and utilizing the DLS/DDLS technique. We could demonstrate that the protein conformational transition and attractive diffusion interactions of monomeric ASN towards a simultaneous assembling and ordering process was triggered only at 50 mM NaCl. Further, the effect of pulsed EFs was investigated and proved to guide ASN assembling and ordering without influencing the protein secondary conformation but accelerating the β-sheet formation. Characterization of physicochemical properties showed in presence of 150 or 250 mM NaCl that the ASN monomers are thermostable and the PEG-induced ASN assemblies show tendency to dissolve and reassemble along with the temperature ramp up and down in a temperature range of 20–70 °C. Mesoscopic ASN assemblies formed at 50 mM NaCl or formed applying pulsed EFs were highly thermostable due to the probably more ordered organization of ASN molecules within the assemblies. More interestingly, pulsed EFs have proved to modify the autofluorescence effect of induced ASN assemblies by adjusting the molecular arrangement and extending the hydrogen-bond networks within assemblies. Especially, we discovered for the first time an extraordinary redshift at 700 nm emission wavelength detected from assemblies formed under the influence of a pulsed EF and applying 250 mM NaCl. Overall, the results presented provide experimental strategies to adjust the kinetics and physicochemical properties of ASN assemblies by applying a NaCl gradient and distinct pulsed EFs.

Conflicts of interest

There are no conflicts to declare.

Acknowledgements

The authors acknowledge financial support by the DFG – project ID BE1443/29-1, by the Cluster of Excellence 'Advanced Imaging of Matter' of the Deutsche Forschungsgemeinschaft (DFG) – EXC 2056 – project ID 390715994, BMBF *via* projects 05K19GU4 and 05K16GUA, and by the China Scholarship Council – project ID [2020]71. The TEM part of work was supported by the European XFEL GmbH, Schenefeld, Germany.

References

1 M. M. Ouberai, J. Wang, M. J. Swann, C. Galvagnion, T. Guilliams, C. M. Dobson and M. E. Welland, *J. Biol. Chem.*, 2013, **288**, 20883–20895.
2 B. Nuscher, F. Kamp, T. Mehnert, S. Odoy, C. Haass, P. J. Kahle and K. Beyer, *J. Biol. Chem.*, 2004, **279**, 21966–21975.
3 L. Krabben, A. Fassio, V. K. Bhatia, A. Pechstein, F. Onofri, M. Fadda, M. Messa, Y. Rao, O. Shupliakov, D. Stamou, F. Benfenati and V. Haucke, *J. Neurosci.*, 2011, **31**, 18149–18154.
4 J. T. Bendor, T. P. Logan and R. H. Edwards, *Neuron*, 2013, **79**, 1044–1066.
5 A. Zbinden, M. Pérez-Berlanga, P. De Rossi and M. Polymenidou, *Dev. Cell*, 2020, **55**, 45–68.
6 S. Krishnan, E. Y. Chi, S. J. Wood, B. S. Kendrick, C. Li, W. Garzon-Rodriguez, J. Wypych, T. W. Randolph, L. O. Narhi, A. L. Biere, M. Citron and J. F. Carpenter, *Biochemistry*, 2003, **42**, 829–837.
7 Y. J. Guo, H. Xiong, K. Chen, J. J. Zou and P. Lei, *Mol. Psychiatry*, 2022, **27**, 758–770.
8 L. M. A. Oliveira, T. Gasser, R. Edwards, M. Zweckstetter, R. Melki, L. Stefanis, H. A. Lashuel, D. Sulzer, K. Vekrellis, G. M. Halliday, J. J. Tomlinson, M. Schlossmacher, P. H. Jensen, J. Schulze-Hentrich, O. Riess, W. D. Hirst, O. El-Agnaf, B. Mollenhauer, P. Lansbury and T. F. Outeiro, *npj Parkinson's Dis.*, 2021, **7**, 65.
9 J.-H. Lee, D.-S. Yang, C. N. Goulbourne, E. Im, P. Stavrides, A. Pensalfini, H. Chan, C. Bouchet-Marquis, C. Bleiwas, M. J. Berg, C. Huo, J. Peddy, M. Pawlik, E. Levy, M. Rao, M. Staufenbiel and R. A. Nixon, *Nat. Neurosci.*, 2022, **25**, 688–701.
10 S. Ray, N. Singh, R. Kumar, K. Patel, S. Pandey, D. Datta, J. Mahato, R. Panigrahi, A. Navalkar, S. Mehra, L. Gadhe, D. Chatterjee, A. S. Sawner, S. Maiti, S. Bhatia, J. A. Gerez, A. Chowdhury, A. Kumar, R. Padinhateeri, R. Riek, G. Krishnamoorthy and S. K. Maji, *Nat. Chem.*, 2020, **12**, 705–716.
11 A. S. Sawner, S. Ray, P. Yadav, S. Mukherjee, R. Panigrahi, M. Poudyal, K. Patel, D. Ghosh, E. Kummerant, A. Kumar, R. Riek and S. K. Maji, *Biochemistry*, 2021, **60**, 3676–3696.
12 P. Alam, L. Bousset, R. Melki and D. E. Otzen, *J. Neurochem.*, 2019, **150**, 522–534.
13 T. M. Krygowski, *J. Chem. Inf. Comput. Sci.*, 1993, **33**, 70–78.
14 M. Tashiro, M. Kojima, H. Kihara, K. Kasai, T. Kamiyoshihara, K. Uéda and S. Shimotakahara, *Biochem. Biophys. Res. Commun.*, 2008, **369**, 910–914.

15 M. A. Saraiva, *Int. J. Biol. Macromol.*, 2021, **177**, 392–400.
16 K. A. Conway, S. J. Lee, J. C. Rochet, T. T. Ding, R. E. Williamson and P. T. Lansbury, *Proc. Natl. Acad. Sci. U. S. A.*, 2000, **97**, 571–576.
17 D. M. Walsh, A. Lomakin, G. B. Benedek, M. M. Condron and D. B. Teplow, *J. Biol. Chem.*, 1997, **272**, 22364–22372.
18 R. Kayed, E. Head, J. L. Thompson, T. M. McIntire, S. C. Milton, C. W. Cotman and C. G. Glabel, *Science*, 2003, **300**, 486–489.
19 I. Benilova, E. Karran and B. De Strooper, *Nat. Neurosci.*, 2012, **15**, 349–357.
20 F. Hasecke, T. Miti, C. Perez, J. Barton, D. Schölzel, L. Gremer, C. S. R. Grüning, G. Matthews, G. Meisl, T. P. J. Knowles, D. Willbold, P. Neudecker, H. Heise, G. Ullah, W. Hoyer and M. Muschol, *Chem. Sci.*, 2018, **9**, 5937–5948.
21 G. P. Concepcion and E. A. Padlan, *Med. Hypotheses*, 2010, **74**, 27–28.
22 S. Ray, T. O. Mason, L. Boyens-Thiele, N. Jahnke and A. K. Buell, *BioRxiv*, 2022, 490467.
23 J. Berry, C. P. Brangwynne and M. Haataja, *Rep. Prog. Phys.*, 2018, **81**, 046601.
24 G. Madras and B. J. McCoy, *J. Chem. Phys.*, 2002, **117**, 8042–8049.
25 J. Stetefeld, S. A. McKenna and T. R. Patel, *Biophys. Rev.*, 2016, **8**, 409–427.
26 B. G. Wilhelm, S. Mandad, S. Truckenbrodt, K. Kröhnert, C. Schäfer, B. Rammner, S. J. Koo, G. A. Claßen, M. Krauss, V. Haucke, H. Urlaub and S. O. Rizzoli, *Science*, 2014, **344**, 1023–1028.
27 C. R. Bodner, C. M. Dobson and A. Bax, *J. Mol. Biol.*, 2009, **390**, 775–790.
28 E. I. Yakupova, L. G. Bobyleva, I. M. Vikhlyantsev and A. G. Bobylev, *Biosci. Rep.*, 2019, **39**, BSR20181415.
29 R. Khurana, V. N. Uversky, L. Nielsen and A. L. Fink, *J. Biol. Chem.*, 2001, **276**, 22715–22721.
30 B. Frieg, L. Gremer, H. Heise, D. Willbold and H. Gohlke, *Chem. Commun.*, 2020, **56**, 7589–7592.
31 C. W. Chung, A. D. Stephens, E. Ward, Y. Feng, M. J. Davis, C. F. Kaminski and G. S. Kaminski Schierle, *Anal. Chem.*, 2022, **94**, 5367–5374.
32 D. Pinotsi, L. Grisanti, P. Mahou, R. Gebauer, C. F. Kaminski, A. Hassanali and G. S. Kaminski Schierle, *J. Am. Chem. Soc.*, 2016, **138**, 3046–3057.
33 A. D. Stephens, M. N. Qaisrani, M. T. Ruggiero, G. D. Mirón, U. N. Morzan, M. C. González Lebrero, S. T. E. Jones, E. Poli, A. D. Bond, P. J. Woodhams, E. M. Kleist, L. Grisanti, R. Gebauer, J. A. Zeitler, D. Credgington, A. Hassanali and G. S. Kaminski Schierle, *Proc. Natl. Acad. Sci. U. S. A.*, 2021, **118**, e2020389118.
34 D. A. Malencik and S. R. Anderson, *Amino Acids*, 2003, **25**, 233–247.
35 R. A. Chica, M. M. Moore, B. D. Allen and S. L. Mayo, *Proc. Natl. Acad. Sci. U. S. A.*, 2010, **107**, 20257–20262.
36 M. Grelich-Mucha, A. M. Garcia, V. Torbeev, K. Ożga, Ł. Berlicki and J. Olesiak-Bańska, *J. Phys. Chem. B*, 2021, **125**, 5502–5510.
37 D. Ubbiali, M. Fratini, L. Piersimoni, C. H. Ihling, M. Kipping, I. Heilmann, C. Iacobucci and A. Sinz, *Angew. Chem.*, 2022, **134**, 1–6.
38 M. Wang, A. L. C. Barra, H. Brognaro and C. Betzel, *Crystals*, 2022, **12**, 437.
39 S. E. Sanchez, D. R. Whiten, G. Meisl, F. S. Ruggeri, E. Hidari and D. Klenerman, *ChemBioChem*, 2021, **22**, 2867–2871.
40 J. N. Rao, C. C. Jao, B. G. Hegde, R. Langen and T. S. Ulmer, *J. Am. Chem. Soc.*, 2010, **132**, 8657–8668.

